Antenna Separation for Multipath Diversity on Direct-with-Earth Links between a Planetary Body and an Earth Station

Marc Sanchez Net*

ABSTRACT. — This article quantifies the required antenna separation to observe independent multipath fading on direct-with-Earth links between a lander and/or rover on a planetary body (e.g., the Moon) and an Earth station. Using a simple ray-based model valid for operation at high frequencies (S-band and above), we show that the required antenna separation to achieve uncorrelated fading is much larger than the half-a-wavelength value typically cited in the literature. We also show that operation at grazing angles exacerbates the problem, especially in the downlink direction, requiring Earth stations to be separated by hundreds of kilometers to achieve diversity. Therefore, we conclude that dual coverage from Deep Space Network (DSN) antennas within the same deep space complex is unlikely to provide "protection" against multipath effects.

To build confidence in the analytical results presented in this article, we discuss the two empirical data sets available from the Chandrayaan-3 and Intuitive Machines 1 mission. The former is used to show signal correlation at two DSN stations within the same complex (i.e., intra-site channel correlation), while the latter provides information for stations in different DSN sites (inter-site channel correlation).

I. Introduction

Multipath fading is a phenomenon of interest to NASA and other space agencies conducting robotic and human exploration of the lunar South Pole. It is caused by electromagnetic (EM) waves reflecting off the lunar surface when a landed vehicle communicates with Earth at low elevation angles, as is the case with lunar landers and

*Telecom Program and Oversight Office.

The research described in this publication was carried out by the Jet Propulsion Laboratory, California Institute of Technology, under a contract with the National Aeronautics and Space Administration.

rovers in regions close to the lunar South Pole. The result of these reflections, known commonly as a multipath channel, severely degrades the link quality, causing power drops (or fades) that in some cases can be larger than 20 dB.

This article builds upon the model presented in Reference [1] to investigate the issue of spatial diversity in direct-to-Earth (DTE) and direct-from-Earth (DFE) links. The goal is to quantify the spatial separation required for multiple antennas to experience uncorrelated multipath channel realizations, a key factor to understand whether antenna diversity is an effective mitigation technique for multipath at planetary distances, and whether co-located antennas in a Deep Space Network (DSN) complex can provide hot backup capability to build resilience against multipath effects.

A secondary use for this article's results is to inform the modeling accuracy needed to predict or reconstruct the interference pattern typically observed in a multipath fading channel. Effectively, it bounds the accuracy with which an analyst would need to know the position of the transmit and receive antennas, and the point of reflection, to be able to estimate both the cadence and the exact timing of the multipath-induced fades.

The rest of this article is structured as follows: First, a brief summary of the model assumed in this article is presented. Then, the issue of spatial separation to achieve antenna diversity is studied first in the downlink direction (from a landed spacecraft to Earth) and then in the uplink direction. Finally, empirical data collected from using the DSN and the Intuitive Machines 1 (IM-1) lander is presented.

A. Preliminaries: System Model for a Single Reflection

This article considers the system model presented in Reference [1], which is based on a single prominently coherent reflection occurring close to the lunar vehicle (see Figure 1). Because I assume operation at S-band or higher, the EM waves are well modeled by rays departing the transmitter and arriving at the receiver either via the direct line-of-sight (LoS) ray or via the surface reflection. The times at which these rays depart, reflect, and arrive are denoted by t_1, t_2, and t_3 for the LoS ray, and t'_1, t'_2, and t'_3 for the reflected ray (see Figure 1).

Using this model, I show in Reference 1 that the state (either in fade or not) of the link between a landed vehicle and an Earth station is determined by the phase difference between the LoS and reflected rays:

$$\Delta\phi(t_3) = 2\pi f_c \Delta\tau_{13} \tag{1}$$

where $\Delta\tau_{13} = \tau_{13} - \tau'_{13}$, $\tau_{13} = t_3 - t_1$ is the total propagation delay over the LoS path, and $\tau'_{13} = t_3 - t'_1 = \tau_{12} + \tau_{23}$ is the same quantity for the reflection path. Furthermore, if we assume a planetary reflection close to the landed vehicle, and propagation in free

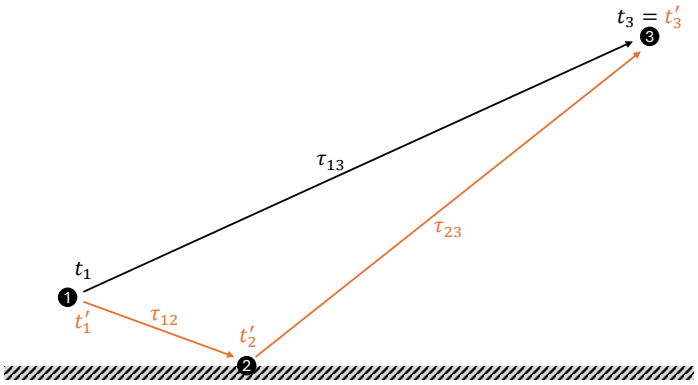

Figure 1. Model of a single coherent reflection in a downlink from a landed spacecraft to an Earth station. Indices 1, 2, and 3 are used to denote the transmitter, point of reflection, and receiver, respectively. Reprinted from Reference 1.

space, the time delays required to evaluate Equation (1) can be approximated as

$$\tau_{13}(t_1, t_3) = \frac{r_{13}}{c} \approx \frac{1}{c}|\vec{\boldsymbol{r}}_3(t_3) - \vec{\boldsymbol{r}}_1(t_1)|, \tag{2}$$

$$\tau_{12}(t_1', t_2') \approx \frac{r_{12}}{c} = \frac{1}{c}|\vec{\boldsymbol{r}}_2(t_1) - \vec{\boldsymbol{r}}_1(t_1)| \tag{3}$$

$$\tau_{23}(t_2', t_3) \approx \frac{r_{23}}{c} = \frac{1}{c}|\vec{\boldsymbol{r}}_3(t_1) - \vec{\boldsymbol{r}}_2(t_1)|, \tag{4}$$

with $r_i(t)$ denoting the position of the transmitter, point of reflection, and receiver in a common frame of reference at time t. Note that these expressions are all approximations because, when tracing the path followed by the reflection ray, the position of the transmitter and point of reflection should be evaluated at t_1' and t_2', respectively. However, I assume that the distance between the transmitter and the reflection point is short enough so that the difference between $r_1(t_1')$ and $r_1(t_1)$ is negligible, and so is the difference between $r_2(t_2')$ and $r_2(t_1)$.

II. Spatial Diversity for Downlinks

A. Theoretical Analysis

To understand the spatial separation needed in the downlink direction, assume that a vehicle landed on a planetary body is transmitting to two Earth stations that are simultaneously receiving the signal.[1] Assume also that because the reflection occurs close to the landed vehicle, its location on the planetary surface can be approximated as the same for both Earth stations.

Figure 2 plots the different electromagnetic rays involved in the system and summarizes the timing relationships that relate their departure and arrival times. Without loss of generality, I assume that t_3 is the reference time for the analysis and express all other events relative to it, with τ_{ij} representing the propagation delays.

[1] Extension to more than two stations receiving is straightforward but not provided for simplicity.

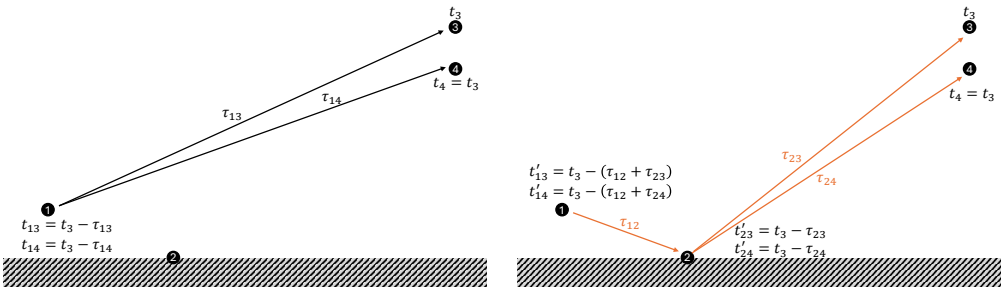

(a) Direct line of sight rays. **(b) Reflected rays.**

Figure 2. Illustration of the reflection geometry. Index 1 denotes the transmitter, 2 denotes the reflection point, and 3 and 4 denote the receiving stations on Earth.

To understand the state of the channels between the transmitter and each Earth station, assume that the transmitter sends a single tone with constant frequency f_c. Following the same reasoning as in Reference [1], the phase of the electromagnetic wave satisfies the following conditions

$$\phi_3(t_3) = \phi_1(t_{13}) \tag{5}$$
$$\phi_4(t_3) = \phi_1(t_{14}) \tag{6}$$
$$\phi'_3(t_3) = \phi_1(t'_{13}) \tag{7}$$
$$\phi'_4(t_3) = \phi_1(t'_{14}), \tag{8}$$

where quantities with the prime symbol are related to the reflected rays, and those without are related to the direct line-of-sight rays. Therefore, the difference in phase between the two EM rays arriving to station 3 is

$$\begin{aligned}\Delta\phi_3(t_3) =& \phi'_3(t_3) - \phi_3(t_3)\\ =& \phi_1(t'_{13}) - \phi_1(t_{13})\\ =& 2\pi f_c\,(t'_{13} - t_{13})\\ =& 2\pi f_c\,[(t_3 - \tau_{12} - \tau_{23}) - (t_3 - \tau_{13})]\\ =& 2\pi f_c\,[\tau_{13} - (\tau_{12} + \tau_{23})]\,.\end{aligned} \tag{9}$$

Next, I assume that the propagation delays can be well approximation by a wave propagating in free space and let $\lambda = \frac{c}{f_c}$ denote the carrier wavelength, with c equal to the speed of light in the vacuum. Then,

$$\begin{aligned}\Delta\phi_3(t_3) \approx& \frac{2\pi}{\lambda}\left[|\vec{\boldsymbol{r}}_3(t_3) - \vec{\boldsymbol{r}}_1(t_{13})| - |\vec{\boldsymbol{r}}_2(t'_{23}) - \vec{\boldsymbol{r}}_1(t'_{13})| - |\vec{\boldsymbol{r}}_3(t_3) - \vec{\boldsymbol{r}}_2(t'_{23})|\right]\\ \approx& \frac{2\pi}{\lambda}\left[(\vec{\boldsymbol{r}}_2(t'_{23}) - \vec{\boldsymbol{r}}_1(t_{13}))\cdot\hat{\boldsymbol{r}}_3(t_3) - |\vec{\boldsymbol{r}}_2(t'_{23}) - \vec{\boldsymbol{r}}_1(t'_{13})|\right],\end{aligned} \tag{10}$$

where the second equality follows from applying the far-field approximation to the fields radiating to Earth. This expression can be further simplified by noting that $\vec{\boldsymbol{r}}_1(t'_{13}) \approx \vec{\boldsymbol{r}}_1(t_{13})$ and $\vec{\boldsymbol{r}}_2(t'_{23}) \approx \vec{\boldsymbol{r}}_2(t_{13})$ because the reflection occurs close to the transmitter and, consequently, the planetary motion between t_{13}, t'_{13}, and t'_{23} can be

neglected. This results in

$$\Delta\phi_3(t_3) \approx \frac{2\pi}{\lambda} r_{12}(t_{13}) \left[\hat{\boldsymbol{r}}_{12}(t_{13}) \cdot \hat{\boldsymbol{r}}_3(t_3) - 1 \right], \tag{11}$$

where $\vec{\boldsymbol{r}}_{12}(t) = \vec{\boldsymbol{r}}_2(t) - \vec{\boldsymbol{r}}_1(t)$ and $r_{12}(t) = |\vec{\boldsymbol{r}}_{12}(t)|$. The exact same reasoning can be applied to the link between the transmitter and station 4, resulting in

$$\Delta\phi_4(t_3) \approx \frac{2\pi}{\lambda} r_{12}(t_{14}) \left[\hat{\boldsymbol{r}}_{12}(t_{14}) \cdot \hat{\boldsymbol{r}}_4(t_3) - 1 \right]. \tag{12}$$

To understand if stations 3 and 4 see different states of the multipath channel, let us consider the following quantity

$$\Delta(t_3) = \Delta\phi_4(t_3) - \Delta\phi_3(t_3) \approx \frac{2\pi}{\lambda} \vec{\boldsymbol{r}}_{12}(t_{13}) \cdot \left[\hat{\boldsymbol{r}}_4(t_3) - \hat{\boldsymbol{r}}_3(t_3) \right], \tag{13}$$

where the approximation follows from assuming that $\vec{\boldsymbol{r}}_{12}(t_{13}) \approx \vec{\boldsymbol{r}}_{12}(t_{14})$ because the planetary motion occurs at scales much slower than the speed of light and, consequently, the time difference $t_{13} - t_{14}$ can be neglected.

Without loss of generality, assume that at an arbitrary moment in time station 3 is experiencing a deep fade (i.e., $\Delta\phi_3(t_3) = \pm 180°$). Then, station 4 is said to experience uncorrelated fading if $\Delta\phi_4(t_3) = 0°$ and, consequently, the channel is in a state of positive interference. In other words, stations 3 and 4 are uncorrelated if

$$\Delta(t_3) = \pm k\pi \;\; k \in \mathcal{N} \tag{14}$$

or, equivalently, if

$$\vec{\boldsymbol{r}}_{12}(t_{13}) \cdot \left[\hat{\boldsymbol{r}}_4(t_3) - \hat{\boldsymbol{r}}_3(t_3) \right] = \pm k \frac{\lambda}{2} \;\; k \in \mathcal{N}. \tag{15}$$

Let (ϵ_3, φ_3) and (ϵ_4, φ_4) denote the position of stations 3 and 4 at time t_3, respectively, expressed relative to a topocentric frame fixed to the transmitter and using spherical coordinates.[2] Then,

$$\begin{aligned} \hat{\boldsymbol{r}}_4(t_3) - \hat{\boldsymbol{r}}_3(t_3) = &\left[\cos\epsilon_4 \cos\varphi_4 - \cos\epsilon_3 \cos\varphi_3\right] \hat{\boldsymbol{x}} \\ &+ \left[\cos\epsilon_4 \sin\varphi_4 - \cos\epsilon_3 \sin\varphi_3\right] \hat{\boldsymbol{y}} \\ &+ \left[\sin\epsilon_4 - \sin\epsilon_3\right] \hat{\boldsymbol{z}} \end{aligned} \tag{16}$$

and

$$\vec{\boldsymbol{r}}_{12}(t_{13}) = r_{12} \left[\cos\epsilon_2 \cos\varphi_2 \hat{\boldsymbol{x}} + \cos\epsilon_2 \sin\varphi_2 \hat{\boldsymbol{y}} + \sin\epsilon_2 \hat{\boldsymbol{z}} \right] \tag{17}$$

so that

$$\begin{aligned} \vec{\boldsymbol{r}}_{12}(t_{13}) \cdot \left[\hat{\boldsymbol{r}}_4(t_3) - \hat{\boldsymbol{r}}_3(t_3)\right] = &\cos\epsilon_2 \left[\cos\epsilon_4 \cos(\varphi_2 - \varphi_4) - \cos\epsilon_3 \cos(\varphi_2 - \varphi_3)\right] \\ &+ \sin\epsilon_2 \left[\sin\epsilon_4 - \sin\epsilon_3\right]. \end{aligned} \tag{18}$$

---

[2] In this article, elevation ϵ is measured with respect to the XY plane of the topocentric frame, rather than using colatitude, so transformation between rectangular and spherical coordinates is adjusted accordingly.

In most reflection geometries dominated by specular reflections, we may assume that the transmitter, reflection point, and Earth are approximately coaligned in azimuth so that $\varphi_2 \approx \varphi_3 \approx \varphi_4$. Then, using basic trigonometric identities results in

$$\vec{\boldsymbol{r}}_{12}(t_{13}) \cdot [\hat{\boldsymbol{r}}_4(t_3) - \hat{\boldsymbol{r}}_3(t_3)] \approx 2 \sin\left(\frac{\epsilon_4 - \epsilon_3}{2}\right) \sin\left(\epsilon_2 - \frac{\epsilon_4 + \epsilon_3}{2}\right), \tag{19}$$

which can be further simplified by noting that at planetary distances $\epsilon_3 \approx \epsilon_4$ to obtain[3]

$$2 \sin\left(\frac{\epsilon_4 - \epsilon_3}{2}\right) \approx \epsilon_4 - \epsilon_3 = \epsilon_{34} \tag{20}$$

$$\sin\left(\epsilon_2 - \frac{\epsilon_4 + \epsilon_3}{2}\right) \approx \sin(\epsilon_2 - \epsilon_3) = -\sin\epsilon_{23}. \tag{21}$$

This leads to the conclusion that

$$\vec{\boldsymbol{r}}_{12}(t_{13}) \cdot [\hat{\boldsymbol{r}}_4(t_3) - \hat{\boldsymbol{r}}_3(t_3)] \approx -r_{12}\epsilon_{34} \sin\epsilon_{23} \tag{22}$$

and, consequently, the channel state experienced in stations 3 and 4 will be uncorrelated when

$$r_{12}\epsilon_{34} \sin\epsilon_{23} = \mp k \frac{\lambda}{2} \;\; k \in \mathcal{N}. \tag{23}$$

Note that in this expression r_{12} must be evaluated at time t_{13} while the angles ϵ_{34} and ϵ_{23} must be evaluated using the positions of the stations at time t_3 and the position of the reflection point at time t_{13}.

To determine the minimum distance between stations 3 and 4 so that the channel is uncorrelated, I seek a solution to the equation

$$r_{12}|\epsilon_{34}| \sin|\epsilon_{23}| = \frac{\lambda}{2}, \tag{24}$$

where ϵ_{34} is a function of the geodetic distance between stations 3 and 4. For example, consider first a simple model where Earth, as seen from the planetary body, can be approximated as a disk. Then, the distance D_{34} between stations 3 and 4 can be approximated as

$$\tan\frac{|\epsilon_{34}|}{2} = \frac{D_{34}/2}{L}, \tag{25}$$

with L equal to the range from the transmitter to the Earth's center. Because $D_{34} \ll L$, we may invoke the small angle approximation to obtain

$$|\epsilon_{34}| \approx \frac{D_{34}}{L} \tag{26}$$

which, upon substitution into Equation (24), results in

$$D_{34} \gtrsim \frac{\lambda}{2} \frac{L}{r_{12} \sin|\epsilon_{23}|}. \tag{27}$$

---

[3] As an example, Earth's angular diameter as seen from a vehicle landed on the Moon is only 2°, approximately. Reflections from planetary bodies located farther away would result in even smaller angular differences.

Note the following remarks:

- This expression is a lower bound on the distance between the stations because it considers Earth as a flat disk. In reality, the geodetic distance will be greater to account for the Earth's curvature.
- This expression shows that D_{34} is proportional to $\lambda/2$, as is commonly stated in the literature.
- The correction factor $\frac{L}{r_{12}\sin|\epsilon_{23}|}$ results in a very large increase in the required antenna separation, driven by two factors: First, the reflection occurs very close to the transmitter so Earth stations see almost identical angles of arrival unless they are vastly separated; and second, operation at grazing angles on the surface of the planetary body results in ϵ_{23} being small, which causes the extra delay of the reflected ray to be small and thus requires stations to be further separated to achieve enough phase difference for the channel to be uncorrelated.

A better solution to Equation (24) can be obtained by assuming that Earth is a perfect sphere and that station 3 and 4 are equally spaced around the transmitter's subsatellite point on Earth.[4] In this case, the angular diameter subtended by the stations as seen from the transmitter is

$$\alpha \approx 2\sin^{-1}\left(\frac{L}{D_E}|\epsilon_{34}|\right) \tag{28}$$

and, consequently,

$$D_{34} = R_E\alpha = D_E\sin^{-1}\left(\frac{L}{D_E}|\epsilon_{34}|\right). \tag{29}$$

Inverting this equation, I find that

$$|\epsilon_{34}| = \frac{D_E}{L}\sin\frac{D_{34}}{D_E} \tag{30}$$

which, upon substitution into Equation (24), results in

$$D_{34} \approx D_E\sin^{-1}\left(\frac{\lambda}{2}\frac{L}{r_{12}D_E\sin|\epsilon_{23}|}\right) \tag{31}$$

B. Numerical Results

I now provide some numerical results to exemplify the orders of magnitude of the antenna separation required to achieve antenna diversity in a direct-to-Earth link between a spacecraft on the lunar surface and the DSN. To parameterize the problem, I assume that the Earth-Moon distance is 485,000 km approximately; that the link

[4] In reality it is unrealistic to assume that stations will be located in such a manner, but the assumption makes sense for the purpose of calculating the *minimum* required station separation.

operates at S-band (2.2 GHz), X-band (8.4 GHz), or K-band (26 GHz); and that the grazing angle ϵ_{23} ranges from 0 to 20 degrees. Figure 3 shows the results of this analysis assuming that the reflection occurs 100 meter away, 1 kilometer away, and 10 kilometers away. To contextualize the distance, horizontal dotted black lines are included, one showing the minimum distance between two DSN complexes, and the other two showing the maximum distance between two antennas within a DSN complex.[5]

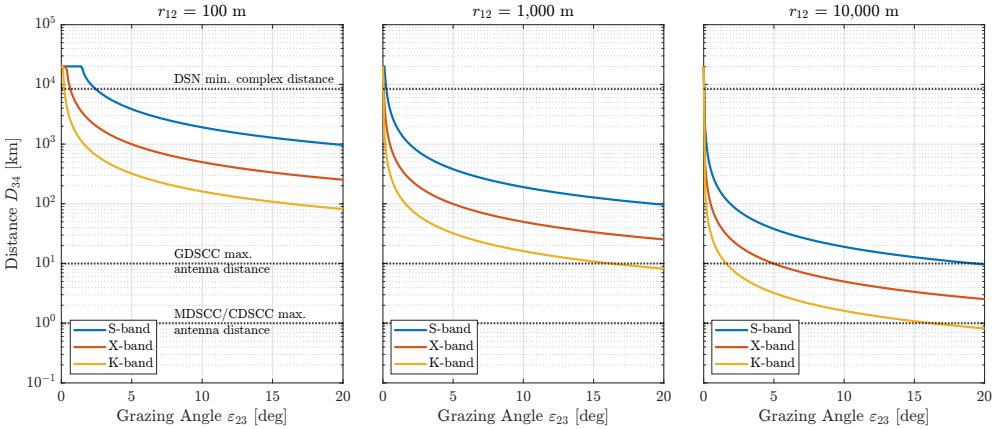

Figure 3. Antenna separation required for a lunar direct-to-Earth link. From left to right, the reflection occurs 100 meters, 1 kilometer, and 10 kilometers away from the lander.

Observe that both the operating band and the distance between the transmitter and the reflection point drive the required station separation on Earth. For example, when the reflection occurs close to the spacecraft (less than 1 km away, approximately) achieving antenna diversity with antennas within a DSN complex is not possible regardless of the band of operation. Therefore, redundancy against multipath effects is only possible during periods of time when two DSN complexes are in view of the spacecraft, or when the DSN is augmented by an affiliated station such as Deep Space Station (DSS) 17 at Morehead State University (MSU). Such a configuration is depicted in Figure 4, which shows the coverage overlap provided by DSS-17 and GDSCC.

When the reflection occurs away from the vehicle, 10 km away or farther, then antenna diversity and hot backup is possible at GDSCC when operating at X- and K-band. However, at MDSCC and CDSCC the antennas are too close to achieve uncorrelated multipath fading channels.

[5]Antennas at the Goldstone Deep Space Communication Complex (GDSCC) can be separated by as much as 10 km, while at Madrid and Canberra the maximum separation is just 1 km approximately.

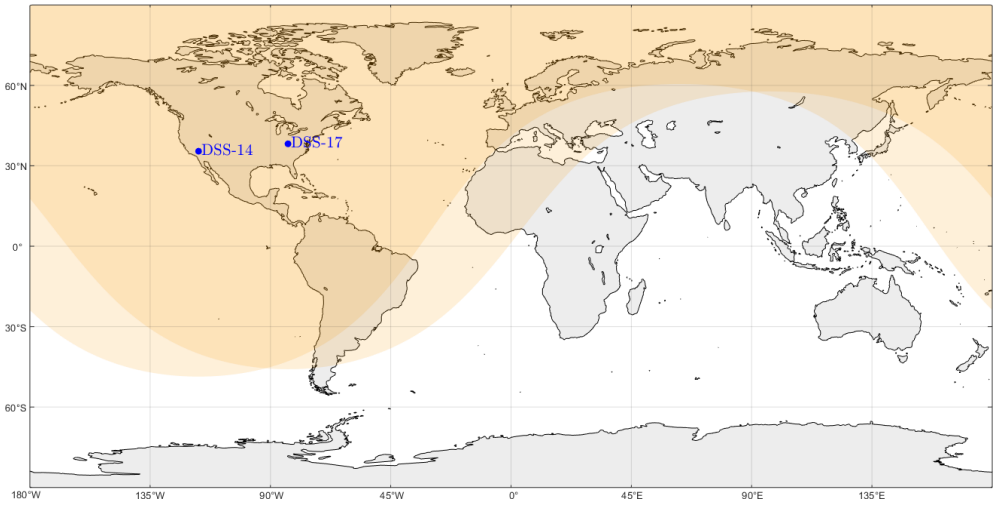

Figure 4. Simultaneous antenna coverage for lunar missions with GDSCC (DSS-14, as an example) and DSS-17 at Morehead State University, Kentucky.

III. Spatial Diversity for Uplinks

A. Theoretical Analysis

I now consider the antenna separation required to achieve antenna diversity for uplinks between an Earth station and a landed spacecraft. In other words, I assume that the vehicle has been fitted with two antennas that are simultaneously receiving the transmission from Earth and are using a combining mechanism to improve the overall system performance. To stay consistent with the nomenclature of Section II, index 1 is used to denote the transmitter (i.e., the Earth station), 2 indicates the reflection point, and 3 and 4 denote the two antennas on board the spacecraft. The resulting geometry, together with the equations relating the different moments in time when EM waves depart or arrive at points of interest is shown in Figure 5.

The theoretical analysis required to obtain the separation D_{34} needed to achieve antenna diversity mirrors that of the downlink. First, the state of the channel between

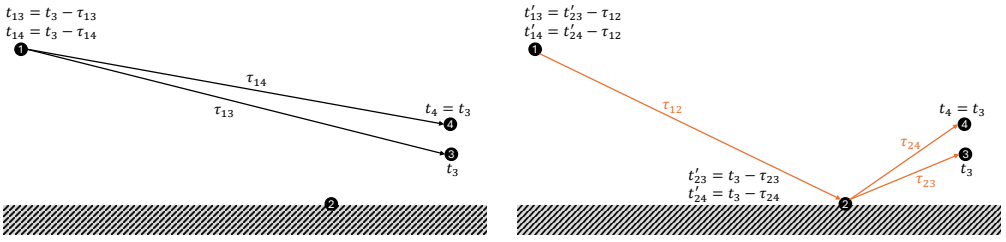

(a) Direct line of sight rays.

(b) Reflected rays.

Figure 5. Illustration of the reflection geometry. Index 1 denotes the transmitter on Earth, 2 indicates the reflection point, and 3 and 4 denote the two receiving antennas on board the landed spacecraft.

the transmitter and each of the antennas is calculated using

$$\Delta\phi_3(t_3) = 2\pi f_c \left[\tau_{13} - (\tau_{12} + \tau_{23})\right] \approx \frac{2\pi}{\lambda}\left[r_{13} - (r_{12} + r_{23})\right] \tag{32}$$

$$\Delta\phi_4(t_3) = 2\pi f_c \left[\tau_{13} - (\tau_{12} + \tau_{24})\right] \approx \frac{2\pi}{\lambda}\left[r_{14} - (r_{12} + r_{24})\right] \tag{33}$$

with

$$r_{13} = |\vec{\boldsymbol{r}}_3(t_3) - \vec{\boldsymbol{r}}_1(t_{13})| \tag{34}$$

$$r_{14} \approx |\vec{\boldsymbol{r}}_4(t_3) - \vec{\boldsymbol{r}}_1(t_{13})| \tag{35}$$

$$r_{12} \approx |\vec{\boldsymbol{r}}_2(t_3) - \vec{\boldsymbol{r}}_1(t_{13})| \tag{36}$$

$$r_{23} \approx |\vec{\boldsymbol{r}}_3(t_3) - \vec{\boldsymbol{r}}_2(t_3)| \tag{37}$$

$$r_{24} \approx |\vec{\boldsymbol{r}}_4(t_3) - \vec{\boldsymbol{r}}_2(t_3)|. \tag{38}$$

Similar to the downlink analysis, these expressions are all approximations that neglect the planetary motion that occurs between different instants in time and simplifies the problem by evaluating all states at times t_{13} and t_3.

Next, we consider the difference in differential phase for each of the channels and obtain

$$\Delta(t_3) = \Delta\phi_4(t_3) - \Delta\phi_3(t_3) \approx \frac{2\pi}{\lambda}\left[(r_{13} - r_{14}) + (r_{23} - r_{24})\right]. \tag{39}$$

The term $r_{13} - r_{14}$ represents the difference in distance in the deep space portion of the link, and it can be simplified by noting that, when operating in a reference frame centered on the landed spacecraft, $r_1 \gg r_3, r_4$ and, consequently

$$r_{13} \approx r_1 - \hat{\boldsymbol{r}}_1 \cdot \vec{\boldsymbol{r}}_3 \tag{40}$$

$$r_{14} \approx r_1 - \hat{\boldsymbol{r}}_1 \cdot \vec{\boldsymbol{r}}_4. \tag{41}$$

Therefore,

$$r_{13} - r_{14} \approx r_{34}\left(\hat{\boldsymbol{r}}_1 \cdot \hat{\boldsymbol{r}}_{34}\right) = D_{34}\left(\hat{\boldsymbol{r}}_1 \cdot \hat{\boldsymbol{r}}_{34}\right). \tag{42}$$

Similarly, the term $r_{23} - r_{24}$ measures the difference in distance from the reflection point to the spacecraft antennas, and its value may be approximated by assuming that at high frequency (S-band and above) the point of reflection is located in the far-field.[6] In other words,

$$r_{23} \approx r_2 - \hat{\boldsymbol{r}}_2 \cdot \vec{\boldsymbol{r}}_3 \tag{43}$$

$$r_{24} \approx r_2 - \hat{\boldsymbol{r}}_2 \cdot \vec{\boldsymbol{r}}_4 \tag{44}$$

and

$$r_{23} - r_{24} \approx r_{34}\left(\hat{\boldsymbol{r}}_2 \cdot \hat{\boldsymbol{r}}_{34}\right) = D_{34}\left(\hat{\boldsymbol{r}}_2 \cdot \hat{\boldsymbol{r}}_{34}\right). \tag{45}$$

---

[6] For an antenna of dimension l, the far-field region starts at distances greater than $2l^2/\lambda$. For example, at S-band and for a ∼10 cm antenna, this critical distance is 15 cm, a value that is much smaller than the tens, hundreds, or thousands of meters away where reflections typically occur.

Combining these results yields

$$\Delta(t_3) \approx \frac{2\pi}{\lambda} D_{34} \left[(\hat{\boldsymbol{r}}_1 - \hat{\boldsymbol{r}}_2) \cdot \hat{\boldsymbol{r}}_{34} \right] \tag{46}$$

which results in a minimum antenna separation distance for antenna diversity given by

$$\frac{2\pi}{\lambda} D_{34} |(\hat{\boldsymbol{r}}_1 - \hat{\boldsymbol{r}}_2) \cdot \hat{\boldsymbol{r}}_{34}| = \pi \tag{47}$$

or, equivalently,

$$D_{34} = \frac{\lambda}{2} \frac{1}{|(\hat{\boldsymbol{r}}_1 - \hat{\boldsymbol{r}}_2) \cdot \hat{\boldsymbol{r}}_{34}|}. \tag{48}$$

Observe that, as for the downlink case, the minimum antenna separation required to experience uncorrelated multipath channels is proportional to $\frac{\lambda}{2}$, as expected, but is also proportional to a factor that depends on the angles of arrival of the line-of-sight and reflected rays. However, unlike the downlink case, neither the distance from Earth to the planetary body nor the distance from the reflection point to the landed spacecraft matter, suggesting that D_{34} will be typically much smaller than in the downlink case (e.g., on the order of tens of centimeters to meters, as opposed to kilometers to tens or hundreds of kilometers). The rationale for this difference between uplink and downlink is clear, it is driven by the fact that the geometry of the reflection is very asymmetric, occurring close to the landed vehicle and really far away from Earth.

To better estimate D_{34}, let the Earth station and the point of reflection be located at coordinates (ϵ_1, φ_1) and (ϵ_2, φ_2), respectively. Without loss of generality, assume that we are working in a topocentric reference frame centered on antenna 3 on board the vehicle, and let (ϵ_4, φ_4) denote the direction toward antenna 4. Then, by definition $\vec{\boldsymbol{r}}_3(t) = 0 \ \forall t$ and

$$\begin{aligned} (\hat{\boldsymbol{r}}_1 - \hat{\boldsymbol{r}}_2) \cdot \hat{\boldsymbol{r}}_{34} = &\cos\epsilon_4 \left[\cos\epsilon_1 \cos(\varphi_1 - \varphi_4) - \cos\epsilon_2 \cos(\varphi_2 - \varphi_4) \right] \\ &+ \sin\epsilon_4 \left[\sin\epsilon_1 - \sin\epsilon_2 \right]. \end{aligned} \tag{49}$$

Similar to the downlink case, we may assume that in most reflection scenarios the Earth station, point of reflection, and antennas on the spacecraft are closely aligned in azimuth so that $\varphi_1 \approx \varphi_2 \approx \varphi_4$. In that case,

$$\begin{aligned} (\hat{\boldsymbol{r}}_1 - \hat{\boldsymbol{r}}_2) \cdot \hat{\boldsymbol{r}}_{34} &= \cos\epsilon_{14} - \cos\epsilon_{24} \\ &= -2 \sin\left(\frac{\epsilon_{14} + \epsilon_{24}}{2} \right) \sin\left(\frac{\epsilon_{14} - \epsilon_{24}}{2} \right) \\ &= -2 \sin\left(\epsilon_{14} - \frac{\epsilon_{12}}{2} \right) \sin\left(\frac{\epsilon_{12}}{2} \right) \end{aligned} \tag{50}$$

with $\epsilon_{ij} = \epsilon_j - \epsilon_i$ equal to the angular difference in the elevation direction. Therefore,

$$D_{34} = \frac{\lambda}{2} \frac{1/2}{|\sin\left(\epsilon_{14} - \frac{\epsilon_{12}}{2}\right) \sin\left(\frac{\epsilon_{12}}{2}\right)|}. \tag{51}$$

To proceed further, we need to make assumptions regarding the geometry of the reflection and the position of the two antennas in the landed vehicle. For example, consider the reflection geometry shown in Figure 6a where the reflection is occurring right in front of the vehicle. In this case $\epsilon_{12} = -2\epsilon_1$ and $\epsilon_{14} = \epsilon_4 - \epsilon_1$ so that

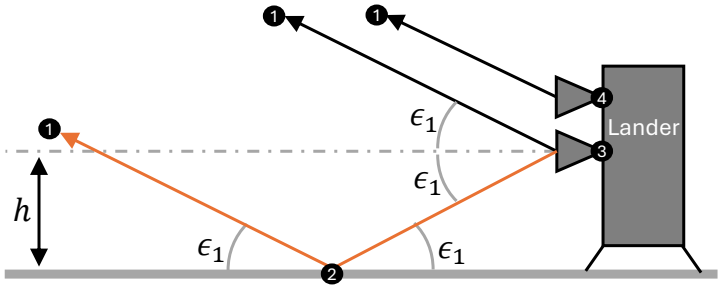

(a) Reflection occurring right in front of the lander.

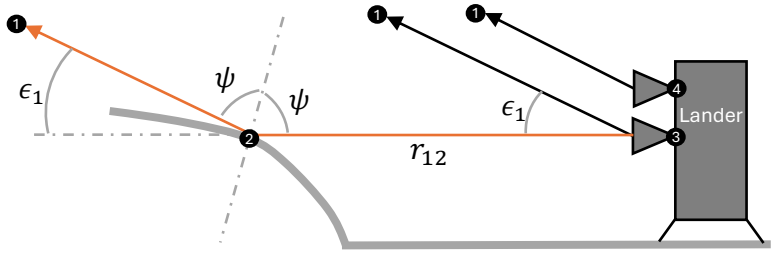

(b) Reflection occurring at a distance, in a slope of a hill or obstacle that is properly oriented for the conditions of specular reflection to be satisfied.

Figure 6. Illustration of two possible reflection mechanisms for a lunar lander communicating with an Earth station (not shown). Distances not to scale.

$$D_{34} = \frac{\lambda}{2} \frac{0.5}{\sin|\epsilon_4| \sin|\epsilon_1|}, \tag{52}$$

which indicates that the required antenna separation is minimized when the two antennas are placed one on top of the other (i.e., $|\epsilon_4| = 90°$) and increases as the elevation angle of the Earth station sets in the lunar sky. In fact, from Equation (51) we see that this last statement is always true regardless of the reflection geometry because operation at very low elevation angles above the terrain implies $\epsilon_{12} \to 0$ and thus $D_{34} \to \infty$.[7]

Next, consider the reflection geometry of Figure 6b. In this case, the angles of the EM rays are such that $\epsilon_{12} = -\epsilon_1$ and, consequently,

$$D_{34} = \frac{\lambda}{2} \frac{0.5}{\sin|\epsilon_4 - \frac{\epsilon_1}{2}| \sin|\frac{\epsilon_1}{2}|}. \tag{53}$$

[7]Evidently the distance D_{34} does not need to be infinitely large to achieve channel diversity. This is a limitation of the far-field approximation, which essentially results in rays being parallel as shown in Figure 6.

We may also consider how the type of vehicle under consideration affects the required antenna separation. For example, for the case of a tall slender lander (e.g., SpaceX's Starship, Intuitive Machine's NOVA-C lander), the antennas are likely to be stacked in the vertical direction and, consequently, $|\epsilon_4| \approx \pi/2$. Therefore

$$|2\sin\left(\tfrac{\pi}{2} - \epsilon_1 - \tfrac{\epsilon_{12}}{2}\right)\sin\left(\tfrac{\epsilon_{12}}{2}\right)| = |\sin\left(\epsilon_1 + \epsilon_{12}\right) - \sin\epsilon_1| = |\sin\epsilon_2 - \sin\epsilon_1| \tag{54}$$

which results in

$$D_{34} \approx \frac{\lambda}{2}\,\frac{1}{|\sin\epsilon_2 - \sin\epsilon_1|} \tag{55}$$

regardless of the exact reflection geometry. Alternatively we may consider a vehicle that has a horizontal deck where antennas are bolted on (e.g., Mars Science Laboratory, Mars 2020). In this case $\epsilon_4 \approx 0°$ and Equation (51) simplifies to

$$D_{34} \approx \frac{\lambda}{2}\,\frac{1}{|\cos\epsilon_2 - \cos\epsilon_1|}. \tag{56}$$

Observe that under the assumption of a flat nearby reflection geometry (see Figure 6a), $\epsilon_2 = -\epsilon_1$ and therefore D_{34} tends to infinity meaning that separating antennas 3 and 4 horizontally never results in uncorrelated multipath channels, regardless of the distance. The physical intuition behind this conclusion is depicted in Figure 7, which shows that the far-field approximation implies that the reflected rays to antennas 3 and 4 are perfectly parallel and thus there is no phase difference between the signals received at each antenna.

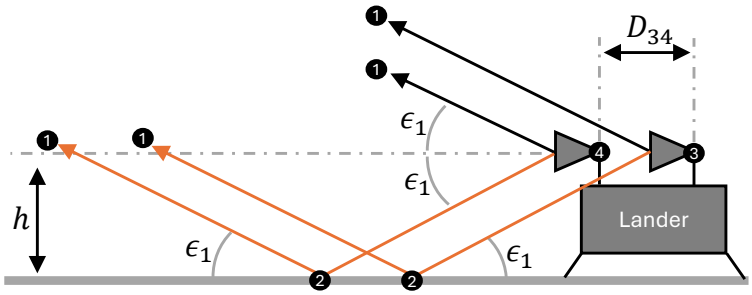

Figure 7. Geometry of the reflection for a flat landing area and a vehicle with two antennas on a flat deck. Under the far-field approximation, all rays are parallel and therefore the channels remain correlated regardless of the separation D_{34}.

B. Numerical Results

This section presents numerical results for the separation required to achieve uplink antenna diversity assuming the reflection geometry shown in Figure 6a, a landed vehicle that can either be tall and slender ($\epsilon_4 \approx 90°$), or similar to a Mars rover with a large horizontal deck. For the latter case, I use $\epsilon_4 = 1°$ to avoid the modeling error incurred when ϵ_4 is exactly zero. Results indicate that except when operating at

extremely low elevation angles ($< 2°$ approximately), it is possible to achieve antenna diversity in the uplink direction by equipping the landed vehicle with two antennas separated by ~ 1 meter or less in the zenith/nadir direction. Furthermore, separating the antennas vertically (in the zenith/nadir direction) is much more efficient than horizontally, which requires separations as large as 10 meters, which are neither practical nor realizable in most cases.

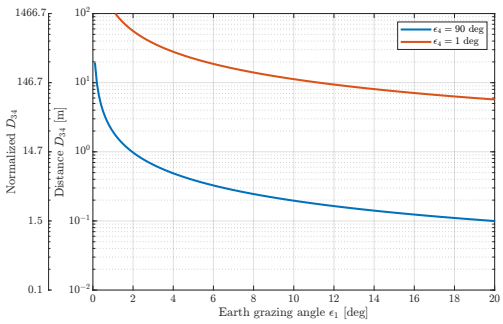

(a) D_{34} at S-band (2.2 GHz).

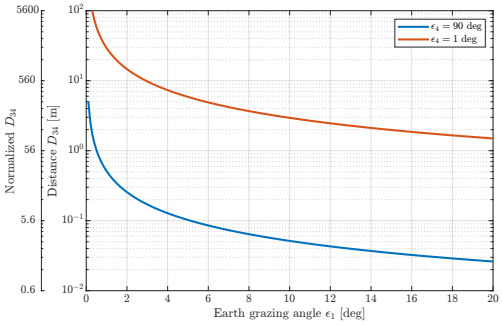

(b) D_{34} at X-band (8.4 GHz).

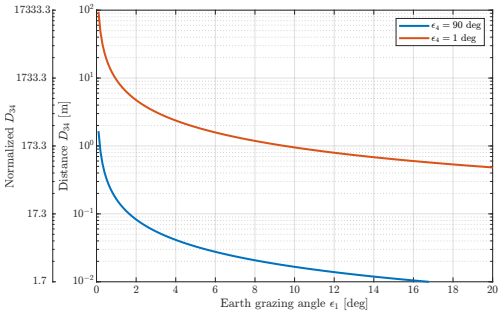

(c) D_{34} at K-band (26 GHz).

Figure 8. Separation between antennas on board a landed vehicle to achieve antenna diversity calculated using Equation (51). $\epsilon_4 = 90°$ indicates that antennas 3 and 4 are stacked vertically, while $\epsilon_4 = 1°$ is representative of the antennas being separated horizontally.

Figure 8 also plots the value of D_{34} normalized by $\lambda/2$, the typical separation quoted in the literature to achieve diversity. Observe that when operating at grazing angles, as is the case for multipath situations such as the lunar South Pole, the actual required separation is $\sim$10 to $\sim$100 times $\lambda/2$. At higher elevations the separation indeed approaches $\lambda/2$, but this is usually a moot point because multipath is no longer a significant effect in the link and, consequently, there is no need for antenna diversity.

Finally, Figure 9 plots the antenna separation needed when $\epsilon_4 = 90°$ depending on whether the reflection geometry is that shown in Figure 6a or Figure 6b. Note that in all cases the reflection from a faraway obstacle (e.g., a ridge, hill, rim of a crater, or similar topographic feature – see Figure 6b) requires larger antenna separation to achieve diversity. However, the difference is not large, on the order of a few tens of centimeters typically, so in practice we conclude that when stacking the two antennas

vertically, the geometry of the experienced reflection is not a driver in the design of the vehicle and telecom system.

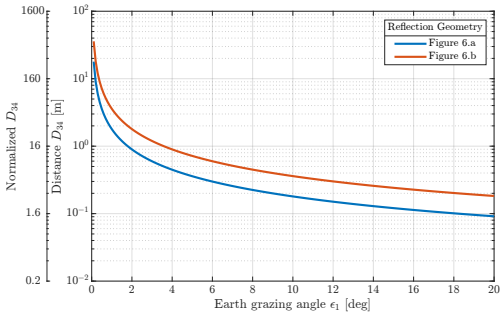

(a) D_{34} at S-band (2.2 GHz).

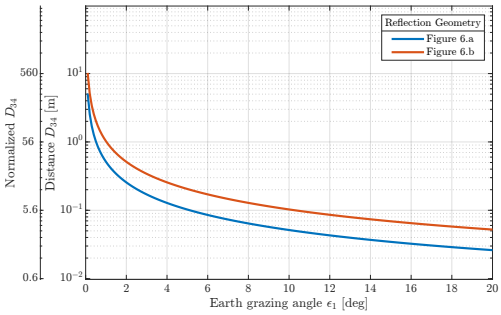

(b) D_{34} at X-band (8.4 GHz).

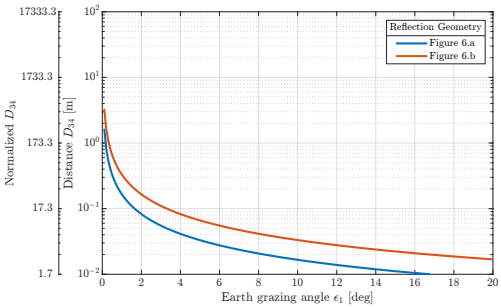

(c) D_{34} at K-band (26 GHz).

Figure 9. Separation between antennas on board a landed vehicle to achieve antenna diversity calculated using Equation (51)**.**

IV. Empirical Data

The DSN has collected empirical data for multipath effects using the Chandrayaan-3 (CH-3) lander, from the Indian Space Research Organisation (ISRO), and using the NOVA-C lander from the Intuitive Machines 1 (IM-1) mission. All collected data were for the downlink direction and at S-band (2.4 GHz, approximately), and only a small fraction of the recordings allow analysis of antenna diversity via simultaneous measurements from multiple DSN sites. Therefore, the data presented here are intended for preliminary results only.

A. Data from the Chandrayaan-3 Lander

DSN provided operational support to the CH-3 lander while in orbit around the Moon, during landing, and for a couple of hours after touchdown. During the powered descent and landing, DSN provided dual coverage with DSS-34 and DSS-36, two 34m beam waveguide (BWG) antennas in the Canberra Deep Space Communications Complex (CDSCC) separated by ~ 500 meters, approximately. Therefore, data from

this mission provided insights for intra-site channel correlation, i.e., the ability of two DSN antennas within the same complex to provide antenna diversity.

Figure 10 plots the symbol signal-to-noise ratio (SSNR) measured by the DSN receivers connected to both antennas during a time window centered around the official landing time. Prior to touchdown, the signal measured at both stations is highly correlated and exhibits oscillations that resemble those experienced during a multipath fading event. However, given that the vehicle was orbiting at ~ 30 kilometers above the surface, it is unclear whether the SSNR fluctuations are due to multipath reflections or to a periodic spacecraft rotation that caused the transmit antenna to operate at off-boresight directions.

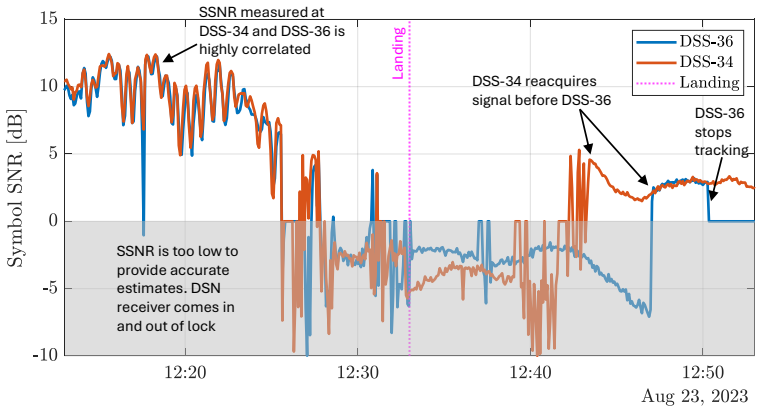

Figure 10. SSNR measurements by the DSN receivers during the CH-3 landing.

During landing, the SSNR level fell below 0 dB, making estimates of the link state unreliable and causing the DSN receiver to lose lock several times. After landing, DSS-34 was the first antenna to reacquire the downlink, followed shortly thereafter by DSS-36. Observe that for a couple of minutes, when both antennas were in lock, the signal once again was highly correlated, thus suggesting that no antenna diversity was experienced.

B. Data from the Intuitive Machines 1 Mission

The IM-1 mission provided a more rich data set to study antenna diversity, with a $\sim$1 hour track with simultaneous measurements from DSS-24 at GDSCC, DSS-36 at CDSCC, and DSS-17 at MSU. For this analysis, I used data power-to-noise spectral density (P_s/N_0) to assess the state of the link, which is derived from open loop recordings obtained at the three stations by first calculating spectrograms and then estimating the carrier power available in the band of interest.

The results of this analysis are shown in Figure 11. Observe that the P_s/N_0 level at DSS-17 is significantly lower than at DSS-24 and DSS-36 because (a) DSS-17 has a 21-meter aperture (instead of a 34-meter dish) and used a room-temperature low noise

amplifier (instead of a cryo-cooled amplifier), and (b) DSS-17 was configured to receive the cross-polarization during the time of interest as requested by IM-1 mission operations.[8]

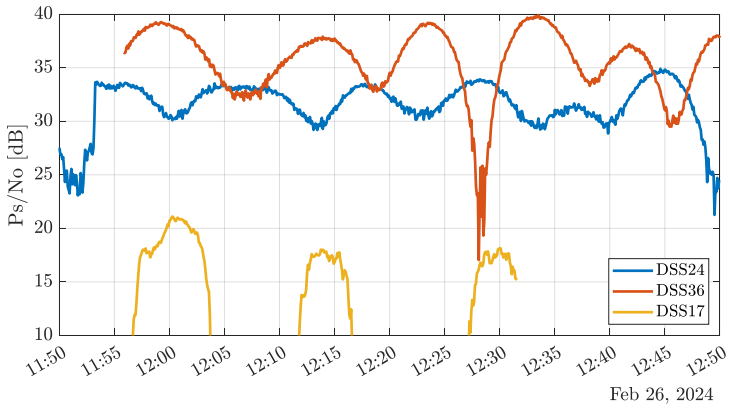

Figure 11. Data SNR (P_s/N_0) derived from open loop recordings.

To gauge the level of correlation between the signal received at the different stations, we may simply look at the timing of the fades experienced at all stations. Observe that DSS-24 and DSS-36 appear to be almost perfectly uncorrelated, with DSS-24 experiencing a fade at the same time that DSS-36 experienced a peak in received gain. This seems to corroborate the analytical results derived in this paper, which predicted that separations on the order of thousands of kilometers are needed at S-band to achieve antenna diversity. Additionally, comparison of DSS-24 and DSS-17 yields an interesting insight: Initially, DSS-17 appeared to be essentially uncorrelated with DSS-24 and perfectly correlated with DSS-36. However, around 12:30, DSS-17 experienced a peak of received power that coincided with a deep fade at DSS-36, and a moment of positive interference at DSS-24. This suggests that regardless of the separation, two Earth antennas will not necessarily remain perfectly uncorrelated forever; instead, their level of correlation will vary with time as the Earth rotates, a fact not properly modeled in the results presented in this paper and that merits further consideration in the future.

V. Conclusions

This article studies the separation needed to achieve antenna diversity in direct-with-Earth links that are affected by multipath fading effects caused by reflections of the EM signal on the planetary body. Using a two-ray model applicable at high frequencies and for predominantly coherent reflections, I derive analytical solutions to estimate:

[8]It is known that specular reflections are stronger in the co-polarization when the reflection occurs at grazing angles (i.e., below the Brewster angle), as is the case in this dataset.

- The separation required so that two Earth stations experience uncorrelated fading channels in a downlink from a landed spacecraft transmitting via a single antenna.
- The separation required for two antennas on board a landed vehicle to experience uncorrelated fading channels in the uplink direction, i.e., when a single Earth station is transmitting.

I show that in both cases the antenna separation is proportional to half of the carrier wavelength, as expected and commonly known in the literature, and depends inversely with the elevation angle of Earth in the lunar sky (i.e., operation at very small grazing angles requires increasingly large antenna separation both on the uplink and downlink). Additionally, in the downlink case the antenna separation is proportional to the distance between the planetary body and Earth, a fact that causes the need for Earth stations to be separated by distances ranging from hundreds of kilometers to one kilometer, depending on the Earth elevation angle in the lunar sky and the distance between the landed vehicle and the point of reflection. Alternatively, in the uplink case, the required antenna separation is mostly driven by the directions of arrival of the direct and reflected waves, and is independent of the distance to the reflection point and the separation between the planetary body and the Earth station. This results in antenna separation values that are much smaller, on the order of tens of centimeters to meters depending on the band of operation, the elevation of Earth in the lunar sky, and the position of the two antennas on the vehicle (whether they are stacked vertically, arranged horizontally, or in some other configuration).

To build confidence in the analytical results, this article presents a small amount of empirical data collected during the CH-3 and IM-1 missions. Using simultaneous measurements from DSN antennas and DSS-17 at MSU, we show that the signal received at two stations separated by ∼500 meters appears to be highly correlated and, consequently, does not provide any resilience against multipath fading effects. Alternatively, simultaneous measurements at DSS-24, DSS-36, and DSS-17 show that support of a lunar mission from different deep space complexes, which are separated by thousands or tens of thousands of kilometers does result in stations experiencing uncorrelated channel states.

A. Future Work

On the analytical front, additional modeling is needed to better understand the effect of Earth's rotation on the channel state between a landed vehicle and two Earth stations. Measurements from IM-1 hint at the fact that Earth's rotation causes the channel to be uncorrelated during certain periods of time, and correlated during others. However, it is unclear whether this relationship is arbitrary, or is related to moments in time when the Moon is rising or setting as seen by the station.

On the empirical front, additional measurements are needed to further corroborate the

findings of this article. As shown in Section IV, only a few hours of real-life data are available to study antenna diversity for planetary multipath links. Therefore, new measurements from upcoming missions headed to the lunar South Pole are required to further solidify the results.

Acknowledgments

The research was carried out at the Jet Propulsion Laboratory (JPL), California Institute of Technology, under a contract with the National Aeronautics and Space Administration (80NM0018D0004).

The author would like to acknowledge the DSN operations team and the staff at MSU's Space Science Center for their support collecting the multipath measurements described in this article. He would also like to acknowledge NASA's Space Communications and Navigation Program (SCaN) for supporting and funding this research. Finally, the author would like to acknowledge Sami Asmar and David Lee of JPL for their thorough technical and editorial review.

References

[1] M. Sanchez Net, "Dynamics of a Coherent Reflection on Direct-with-Earth Links between a Planetary Body and an Earth Station," *The Interplanetary Network Progress Report*, Volume 42-240, Jet Propulsion Laboratory, Pasadena, California, pp. 1-32, February 15, 2025.
https://ipnpr.jpl.nasa.gov/progress_report/42-240/42-240A.pdf